5 Fabrication and Testing of the Cylindrical Telemetry Array

To validate the computer designs presented in the previous chapter, this chapter will present the design, fabrication, and testing of a truncated corner patch telemetry antenna array for a 14-inch cylinder. The design of the omnidirectional circularly polarized telemetry antenna will be based on the material presented in chapter 4. The measured characteristics of interest are the antenna's return loss, polarization, and directivity.

5.1 Antenna Design

The substrate used in the antenna design is RT-Duroid 5870, which was donated to the University of Alaska's electrical engineering department by Rogers Corporation. This substrate has a thickness of 60 mil and a dielectric constant of 2.33, which provides adequate bandwidth and radiation efficiency. Additionally, its flexibility allows the antenna array to be easily wrapped around the cylinder.

The size of the etcher located in the UAF electrical engineering department cannot accommodate substrates larger than approximately 12 inches long. As a result, the antenna array must be divided into four sections. Dividing the array in this manner affects the number of elements in the array and the layout of the L-section matching network. Sixteen elements are chosen for the array because this number simplifies the corporate feed design andallows the array to easily be divided into the four necessary sections. The stub used in the L-section matching network cannot be a single straight

microstrip line, but must be folded to allow the stub to have the required electrical length while still allowing it to fit in the limited space available for each array section.

The design of the truncated corner antenna array was accomplished using Clementine. The array's large surface area requires Clementine to perform many calculations to complete the fullwave analysis of the antenna. To minimize the amount of time required, the overall design of the 16 element antenna array was accomplished in two steps. First, using the dimensions of the truncated corner element designed in chapter 4, a quad-element array section was tuned using Clementine. The final 16-element array, consisting of four quad-element sections, was then tuned. The tuning processes was accomplished by iterating analysis simulations of the array until the antenna's axial ratio was 0 dB at the telemetry frequency of 2.2155 GHz.

The designed array is shown in figure 5.1. The four quad-sections can be seen, each having four antenna elements, as well as the L-section matching networks with folded tuning stubs. The matching networks were designed using 100 ohm impedance transmission lines rather than the 50 ohm lines used in the simulated designs described in chapter 4. The reason for using the 100 ohm impedance lines is they simplified the matching network because no quarter wave transformer matching section is required at the first T-junction. The array dimensions are listed in table 5.1. Clementine's simulated results are shown in figures 5.2 – 5.5. The array is omnidirectional with approximately 1 dB of pattern ripple and an axial ratio of 0.5 dB broadside to the patch. As shown in the results from chapter 4, the axial ratio and gain performance of the patch array degrade away from broadside.

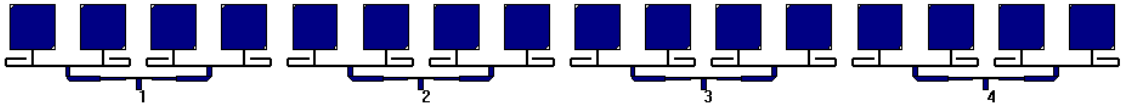

Figure 5.1. 16 element truncated corner, circularly polarized array and matching sections for 14-inch diameter cylinder.

Table 5.1 Patch and matching network dimensions.

Patch Dimensions				L-section Dimensions	
Patch Length	Patch Width	Transmission Line Width	Truncated Corner Side Length	Series Length	Stub Length
(mm)	(mm)	(mm)	(mm)	(mm)	(mm)
43.89	43.89	1.25	4.266	15.875	26.25 + 16.5 + 20.275

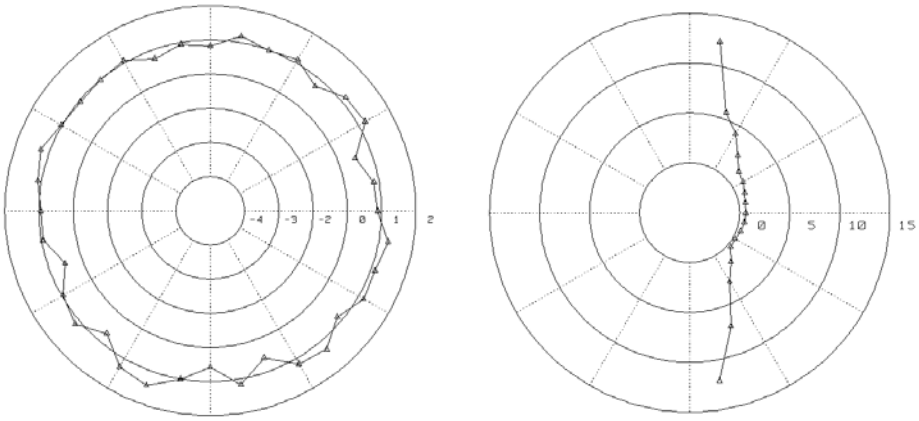

a. azimuth plane **b.** elevation plane

Figure 5.2. Axial ratio performance of circularly polarized array.

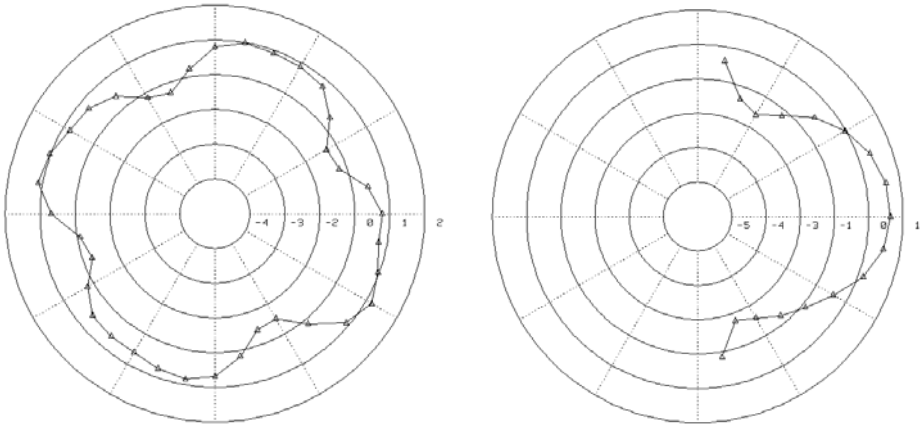

a. azimuth plane **b.** elevation plane

Figure 5.3. Gain performance of circularly polarized array.

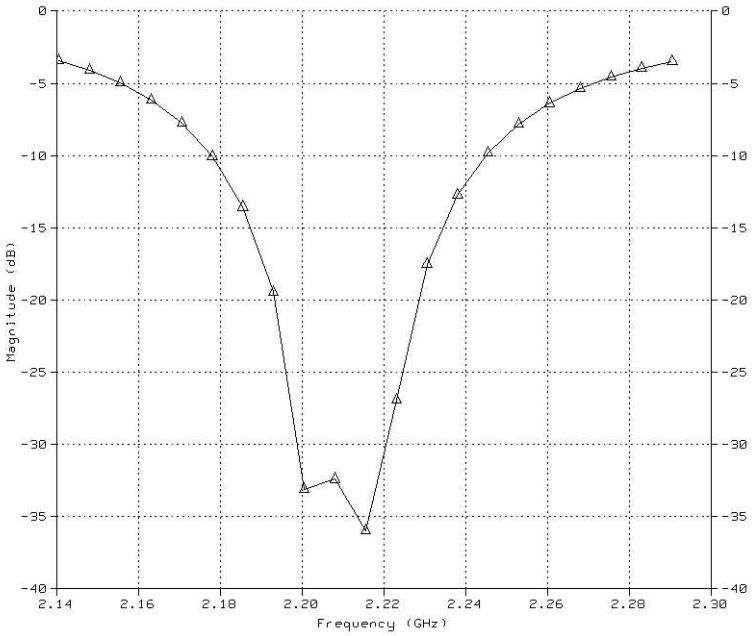

Figure 5.4 S_{11} performance.

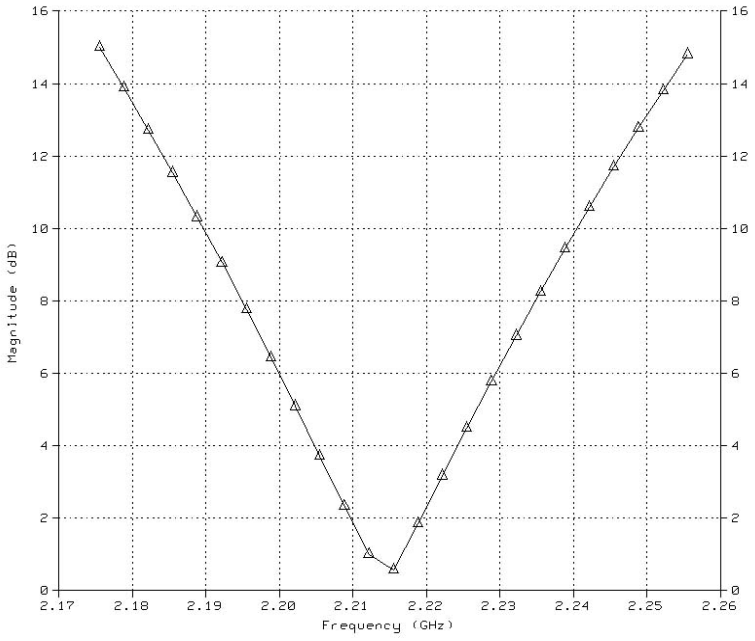

Figure 5.5 Axial ratio performance broadside to cylinder.

5.2 Antenna Fabrication

The antenna was fabricated using materials and equipment available in the UAF electrical engineering department. The substrate used was 60 mil, ½ oz. copper RT-Duroid that was obtained from Rogers Corporation free of charge under their University Program. The fabrication process can be summarized in 7 steps:

1. A negative mask of the antenna is constructed using AutoCAD and printed on a transparency.
2. A photoresist layer is laminated to the top copper layer of the RT-Duroid printed circuit board.
3. The mask is placed over the photoresist, and it is expose to UV light for approximately 6 minutes.
4. A developing process removes the photoresist not exposed to UV light in step three. After developing, the photoresist remains only on the antenna elements and feeding networks.
5. The copper layer without photoresist is stripped off by an etching process, leaving the copper required for the antenna elements and the feeding networks.
6. The photoresist still present on the antenna and feed networks is removed.
7. SMA connectors are soldered to the necessary feed points.

There are two factors that limit the size of the antenna which can fabricated in the engineering department. First, the fabrication size is limited by the size of the mask. If a mask is made using a transparency, the mask size is limited to 8.5 by 11 inches. The advantage of using a transparency is that the mask can be made using any printer. If the mask is made by the UAF printing services, the size of the mask's negative is limited to approximately 14 by 17 inches. The second factor is the size and performance of the etching machine. The maximum size of the RT-Duroid section that can fit within the

etcher is approximately 11 by 14 inches. However, because the spraying mechanism within the etcher can only uniformly spray the etching solution on a 5 by 10 inch surface, the largest antenna size that can be accurately fabricated is approximately 5 by 10 inches. Due to these limiting factors, the antenna array was divided in four sections.

Using AutoCAD, the quad-section mask was designed to fit on an 8.5 by 11 inch transparency. An outline of the mask is shown in figure 5.6. Using this mask, four quad-sections were fabricated using steps 1 through 7 listed above. A fabricated array quad-section is shown in figure 5.7.

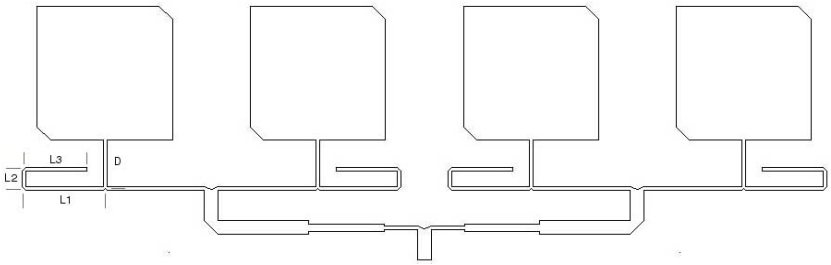

Figure 5.6. Mask of a single quad-section used in the 16 element array (not to scale).

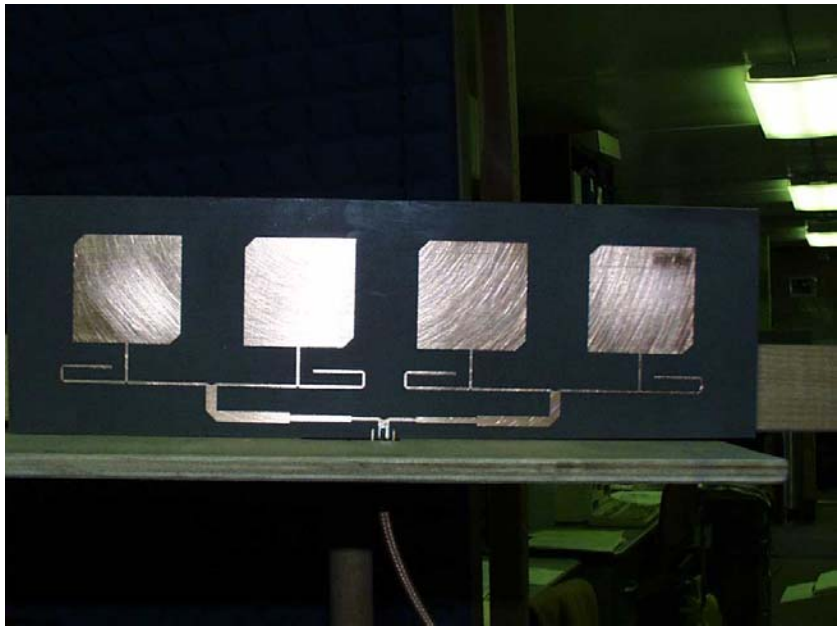

Figure 5.7. Fabricated quad-section.

5.3 Antenna Testing

The fabricated antenna's performance is characterized in this section by measuring its return loss, axial ratio, and radiation pattern. Acceptable measured values are a return loss greater than 10 dB, an axial ratio less than 6 dB, and a radiation pattern ripple less than 3 dB. For the measurements, the designed cylindrical array was used as a receiving antenna. The source antenna was a halfwave dipole. The signal source was generated using either a vector network analyzer or using ASRP's telemetry transmitter. In order to measure the antenna's received signal with a bench top network analyzer or spectrum analyzer, a four-way power divider was required.

5.3.1 Return Loss Measurement

The return loss measurement was accomplished using a vector network analyzer. The measured return loss of the array is shown in figure 5.8. As seen in the figure, the return loss at the operating frequency of 2.2155 GHz is 23 dB and the 3 dB bandwidth is 235 MHz.

5.3.2 Axial Ratio Measurement Technique

By measuring the electric field strength of the antenna, the axial ratio can be determined using the multiple-amplitude-component method [105]. Using this method, the axial ratio can easily be determined by taking four measurements with a dipole and performing several basic calculations. The main limitation using this simple method is that the polarization sense cannot be determined.

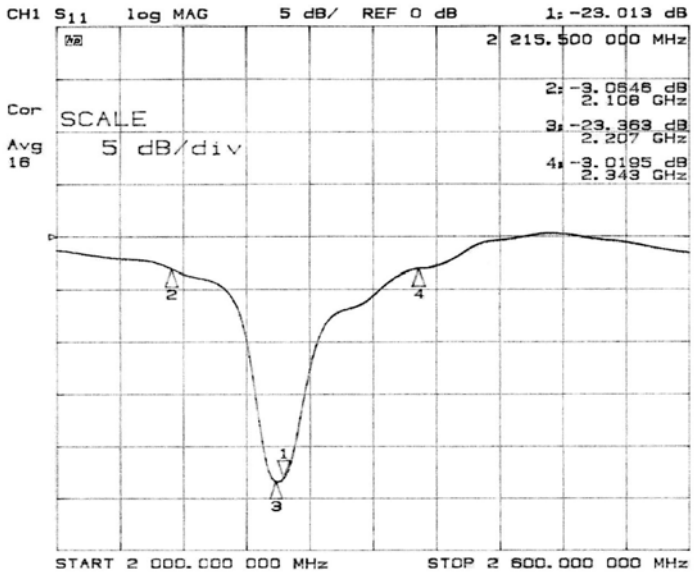

Figure 5.8. Return loss of a single quad-section.

The equations used in the multiple-amplitude-component method are derived from the geometry of the polarization box, which is related to the Poincare Sphere (see figure 5.9). The axial ratio is calculated from electric field measurements taken at four separate angles: 0, 45, 90, and 135 degrees. The measured electric fields are related to

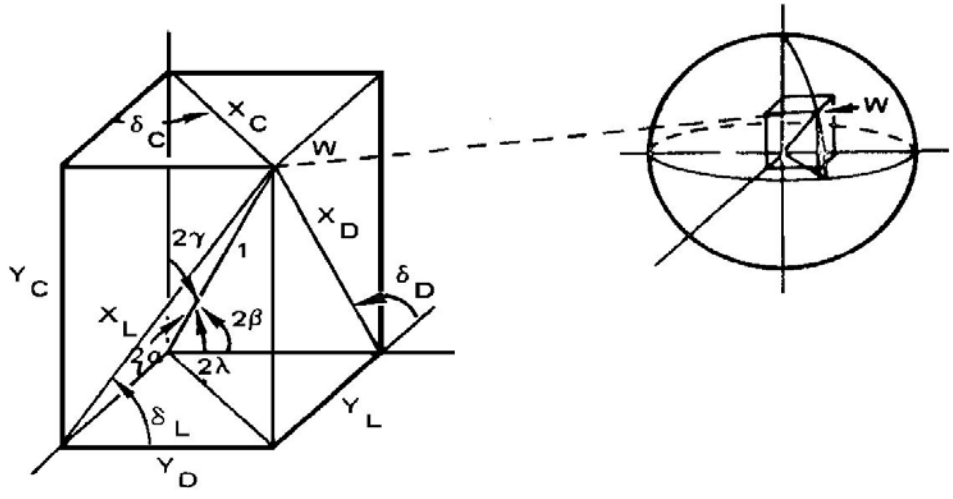

Figure 5.9. Polarization box and its relationship to the Poincare sphere [106].

the polarization box by

$$Y_D = \frac{(1-\rho_D^2)}{(1+\rho_D^2)} \tag{5.1}$$

and

$$Y_L = \frac{(1-\rho_L^2)}{(1+\rho_L^2)} \tag{5.2}$$

where the electric field ratios are given by

$$\rho_L = \frac{E_{90}}{E_0} \tag{5.3}$$

and

$$\rho_D = \frac{E_{135}}{E_{45}} \text{ .} \tag{5.4}$$

Using these relations, the axial ratio can be determine from the measured electric fields by

$$AR_{linear} = \cot\left(\frac{1}{2}\cos^{-1}\left(Y_L^2 + Y_D^2\right)^{1/2}\right) \tag{5.5}$$

For highly accurate axial ratio measurements, a standard dipole should be used. However, the axial ratio measurements reported in this chapter use a half-wavelength dipole constructed using 1 mm copper wire and 50 ohm BNC cable (see figure 5.10a). In order to make the measurements, several cables were needed for both the receive and transmit antenna. To make the four necessary measurements at 0, 45, 90, and 135 degrees, a protractor was attached to the antenna mount. The cross polarized characteristics for this antenna was measured to be -20 to -30 dB using a second half wavelength dipole shown in figure 5.10b.

The electric field measurements of the cylindrical array, required for the axial ratio calculations, were taken at two separate locations. First, the antenna electric fields were tested in the anechoic chamber using a network analyzer (see figure 5.11a). Second, the fields were tested in a field outdoors at the UAF agricultural farm, located between Geist and Sheep Creek Roads, using a spectrum analyzer (see figure 5.11b).

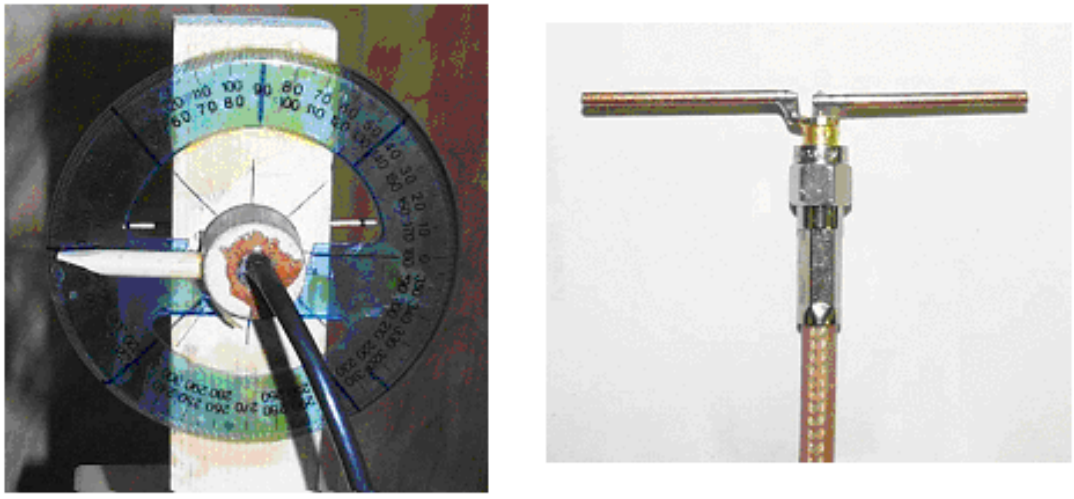

a. rotating dipole attached to BNC cable. **b.** fixed dipole attached to SMA connector.

Figure 5.10. Half-wave dipole antennas used in measurements.

5.3.3 Axial Ratio Measurement using Anechoic Chamber

The electric field strength of the antenna was first measured in the anechoic chamber located in the electrical engineering microwave lab. There are two factors that limited the accuracy of the measurements taken within the anechoic chamber. First, due to a lack of microwave absorbing material, there were large openings on both sides of the chamber. The anechoic chamber had 12 side panels. However, there was only enough absorbing material to cover 10 panels. As a result, two of the 12 side panels were open,

one on each side of the chamber. Figure 5.11a shows a portion of one open side panel. Second, the size of the anechoic chamber was not sufficient to guarantee that the measurements were taken in the farfield defined as

$$R_{farfield} = \frac{2D^2}{\lambda}, \tag{5.6}$$

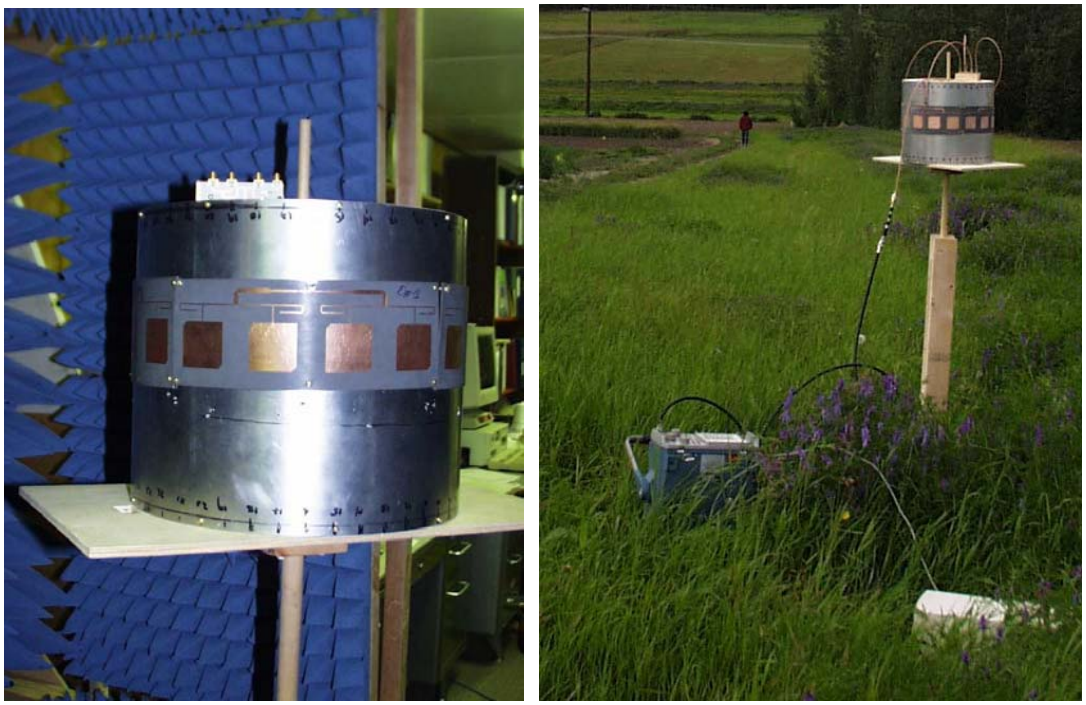

a. anechoic chamber **b.** UAF agricultural farm

Figure 5.11. Radiation pattern testing locations.

where D is maximum dimension of the antenna. For the cylindrical array, the maximum dimension was taken as the diameter of the cylinder. To ensure that the measurements met the farfield requirement, the transmit antenna was placed slightly outside the anechoic chamber. This required that the two end panels be opened slightly, leaving an opening of approximately 4 inches wide. While these openings likely degraded the measurements, the error is assumed to be less than a few dB.

The antenna array was placed in the anechoic chamber as shown in figure 5.11a. The test signal was generated and measured using a vector network analyzer. The signal from the network analyzer was transmitted using the dipole shown in figure 5.10a. The signal was received by the cylindrical array and its signal strength was also measured by the vector network analyzer. The network analyzer S_{21} parameter is a measure of the electric field strengths of the transmitted and received signals. Rotating the transmitting dipole antenna to the necessary angles, S_{21} measurements broadside to the array were recorded. Using equations 5.1 – 5.5, the axial ratio in the azimuth plane was calculated. Three separate axial ratio measurements were made, and the results are plotted in figure 5.12. The average measured values for these three measurements are listed in table 5.2. As seen in the table, the axial ratio at the operating frequency of 2.2155 GHz was measured to be 1.7 dB, which corresponds to a loss of 0.16 dB if a radiated signal from this array is received by a circularly polarized ground station antenna.

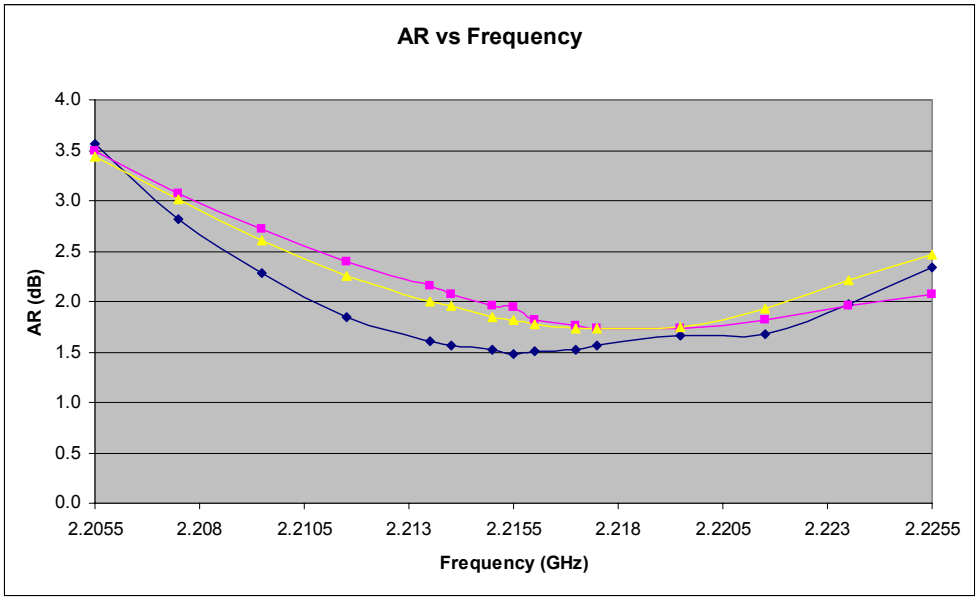

Figure 5.12. Axial ratio measurements taken in anechoic chamber.

Table 5.2. Axial ratio data measured using network analyzer (average of 3 measurements).

Cylinder Test Point	Freq1	Network Analyzer S21 Measurement				AR	Polarization Mismatch Loss
		P0	P45	P90	P135		
	(GHz)	(dB)	(dB)	(dB)	(dB)	(dB)	(dB)
Broadside	2.2055	-41.55	-46.00	-46.22	-41.80	3.48	0.59
Broadside	2.2075	-41.16	-44.92	-45.60	-41.66	2.95	0.44
Broadside	2.2095	-40.65	-43.79	-44.87	-41.43	2.52	0.33
Broadside	2.2115	-40.18	-42.75	-44.13	-41.27	2.15	0.25
Broadside	2.2135	-39.77	-41.87	-43.48	-41.18	1.90	0.20
Broadside	2.2140	-39.71	-41.67	-43.34	-41.21	1.83	0.18
Broadside	2.2150	-39.60	-41.31	-43.08	-41.26	1.74	0.17
Broadside	2.2155	-39.53	-41.20	-42.95	-41.30	1.71	0.16
Broadside	2.2160	-39.58	-41.06	-42.88	-41.39	1.66	0.15
Broadside	2.2170	-39.56	-40.81	-42.72	-41.55	1.63	0.15
Broadside	2.2175	-39.57	-40.70	-42.65	-41.67	1.63	0.15
Broadside	2.2195	-39.76	-40.47	-42.51	-42.23	1.67	0.15
Broadside	2.2215	-40.09	-40.35	-42.12	-42.97	1.70	0.16
Broadside	2.2235	-40.47	-40.33	-42.13	-43.73	1.93	0.20
Broadside	2.2255	-41.02	-40.38	-42.15	-44.50	2.16	0.25

5.3.4 Axial Ratio Measurement using Outdoor Range.

The electric field strength of the antenna was measured outdoors, in a field near UAF (see figure 5.11b). The cylindrical antenna array was used as the receiving antenna, and the dipole shown in figure 5.10a was used as the transmitting antenna. These antennas were separated by 40 feet. The signal source was ASRP's telemetry transmitter, which generated at single tone at 2.2155 GHz. The signal received by the cylindrical array was measured using a spectrum analyzer. The DC power required to operate both the transmitter and the spectrum analyzer were supplied by portable universal power supplies (UPS) which are typically used to back up computers.

The azimuth plane data is plotted in figure 5.13 and tabulated in table 5.3. As seen in the figure, the axial ratio fluctuates in the azimuth plane by approximately +/- 1 dB, with the average axial ratio of approximately 1.5 dB. It should be noted that 0 degrees and 360 degrees are the same point. At this point, the axial ratio measured at this point differ by 1.4 dB. One cause of this discrepancy is likely the rotation of the platform

during the measurements. During the rotation, the many cables used to connect the cylindrical array to the spectrum analyzer experienced movement, causing the cable connections to loosen. Another source of error was that the dipole shown in figure 5.10a was not guaranteed to be exactly at 0, 45, 90, or 135 degrees since there was no locking mechanism on the antenna mount. And finally, the most significant source of error was likely the result of ground reflections.

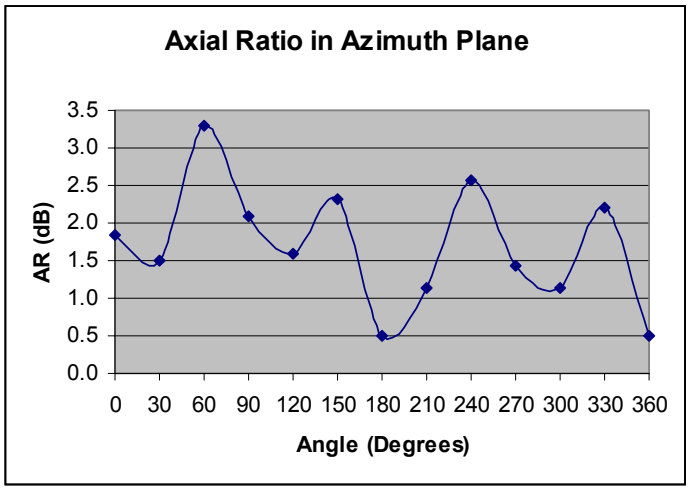

Figure 5.13. Azimuth plane axial ratio measured in outdoor range.

Table 5.3. Azimuth plane axial ratio data measured using spectrum analyzer.

Cylinder Test Point	Azimuth Angle	Spectrum Analyzer Power				AR	Polarization Mismatch Loss
		P0	P45	P90	P135		
	(degrees)	(dBm)	(dBm)	(dBm)	(dBm)	(dB)	(dB)
Broadside	0	-32	-32	-34	-35	1.85	0.19
Broadside	30	-35	-34	-35	-37	1.50	0.13
Broadside	60	-32	-31	-34	-37	3.29	0.53
Broadside	90	-38	-36	-34	-35	3.08	0.23
Broadside	120	-35	-33	-34	-36	1.59	0.14
Broadside	150	-34	-34	-36	-38	2.31	0.28
Broadside	180	-35	-36	-36	-36	0.50	0.01
Broadside	210	-34	-34	-35	-36	1.13	0.07
Broadside	240	-34	-33	-35	-38	2.58	0.35
Broadside	270	-35	-33	-33	-35	1.44	0.12
Broadside	300	-37	-35	-36	-37	1.13	0.07
Broadside	330	-33	-33	-36	-36	2.22	0.26
Broadside	360	-36	-36	-37	-36	0.50	0.01

The measured elevation plane axial ratio data is plotted in figure 5.14 and tabulated in table 5.4. In the figure, the measurements taken broadside to the cylinder correspond to the data plotted at 0, 180, and 360 degrees. The measurements taken at the top and bottom of the cylinder correspond to the data plotted at 90 and 270 degrees, respectively. The measurements show that the axial ratio of the array degrades near the top and bottom of the cylinder.

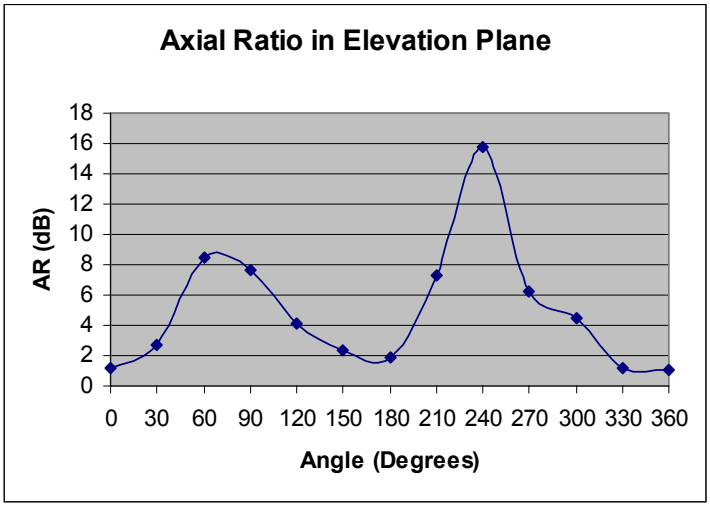

Figure 5.14. Elevation plane axial ratio measured in outdoor range.

Table 5.4. Elevation plane axial ratio data measured using spectrum analyzer.

Cylinder Test Point	Elevation Angle	Spectrum Analyzer Power				AR	Polarization Mismatch Loss
		P0	P45	P90	P135		
	(degrees)	(dBm)	(dBm)	(dBm)	(dBm)	(dB)	(dB)
Broadside	0	-33	-35	-35	-34	1.13	0.07
	30	-33	-37	-36	-33	2.65	0.36
	60	-32	-35	-49	-35	8.50	1.95
Bottom	90	-42	-48	-50	-42	7.59	1.75
	120	-40	-43	-48	-42	4.80	0.76
	150	-31	-32	-35	-34	2.31	0.28
Broadside	180	-33	-35	-36	-33	1.85	0.19
	210	-32	-35	-45	-33	7.28	1.67
	240	-38	-48	-49	-43	15.76	2.79
Top	270	-49	-41	-41	-46	6.24	1.40
	300	-42	-45	-51	-45	4.50	0.89
	330	-34	-34	-36	-35	1.13	0.07
Broadside	360	-34	-34	-36	-34	1.00	0.06

5.3.5 Radiation Pattern Measurement using Outdoor Range.

The radiation pattern is measured to determine the array's directivity. Because the antenna elements are fed with equal amplitudes and phases, and the element spacing is less than a guided wavelength, the radiation pattern is assumed to be omnidirectional. The radiation patterns for both the azimuth and elevation planes were measured using the dipole shown in figure 5.10b. The measurements were taken while keeping the dipole horizontal and rotating the cylindrical array. The test signal was generated using ASRP's telemetry transmitter. The power of the signal received by the cylindrical array was measured using a spectrum analyzer. The azimuth and elevation pattern measurements are tabulated in table 5.5 and plotted in figures 5.15 and 5.16. The pattern ripple in the azimuth plane is seen to be approximately 3 dBm. In the elevation plane, the measured data shows that the signal power degrades by 5 to 15 dBm near the top and bottom regions of the cylinder. In contrast, while the Clementine simulations also showed degraded signal strength away from the antenna's broadside, it predicted that at the extreme angles of +/- 90 degrees, the signal strength would increase.

5.3.6 Comparison of Measured and Simulated Results.

The performance of the measured data is compared to the performance of the simulated data from chapter 4 in table 5.6. The discrepancies most likely are the result of reflections from the ground. Another possible source of error is that the cylinder was not perfectly round.

The measured and simulated S_{11} characteristics are similar, with both have minimum magnitudes near 2.2155 GHz. The axial ratio's center frequency (the frequency where the axial ratio is minimum) is about 2 MHz off from the simulated value. The measured axial ratio listed in the table is an approximation because the minimum measured axial ratio actually flattened out over a wide range of frequencies, rather than linearly approaching a single minimum value as in the simulation results. This flattening is assumed to be a result of the inability to accurately measure the electric fields using the lab equipment and measurement facilities currently available in the microwave lab. More specifically, the accuracy of the measurements are limited by the non-standard dipole antenna, the anechoic chamber's construction, and the ground reflections present in the outdoor range. Although greater than predicted, the axial ratio of 1.7 dB still guarantees low polarization mismatch loss.

Table 5.5. Radiation pattern data measured using dipole in figure 5.9a.

Cylinder Test Point	Azimuth Angle (degrees)	Spectrum Analyzer Power (dBm)
Broadside	0	-32.00
Broadside	30	-32.00
Broadside	60	-31.00
Broadside	90	-33.00
Broadside	120	-30.00
Broadside	150	-33.00
Broadside	180	-31.00
Broadside	210	-32.00
Broadside	240	-32.00
Broadside	270	-31.00
Broadside	300	-33.00
Broadside	330	-31.00
Broadside	360	-32.00

Cylinder Test Point	Elevation Angle (degrees)	Spectrum Analyzer Power (dBm)
Broadside	0	-29.00
	30	-28.00
	60	-31.00
Bottom	90	-47.00
	120	-31.00
	150	-28.00
Broadside	180	-28.00
	210	-29.00
	240	-36.00
Top	270	-33.00
	300	-33.00
	330	-30.00
Broadside	360	-29.00

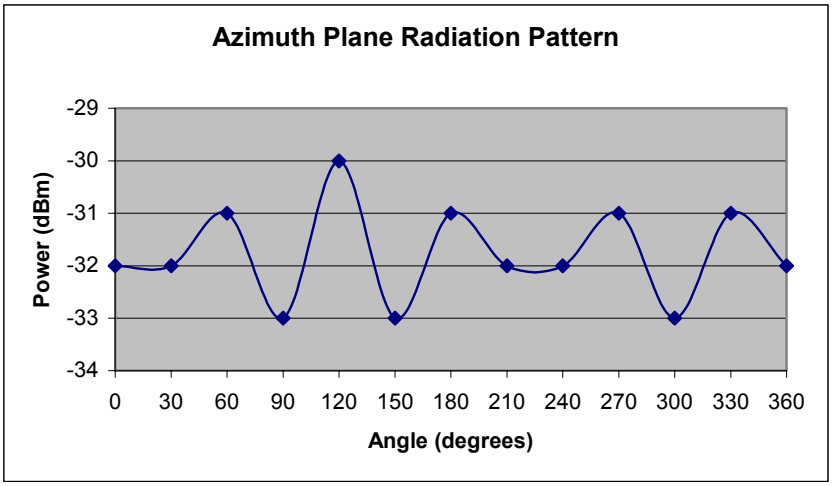

Figure 5.15. Azimuth plane radiation pattern measured in outdoor range.

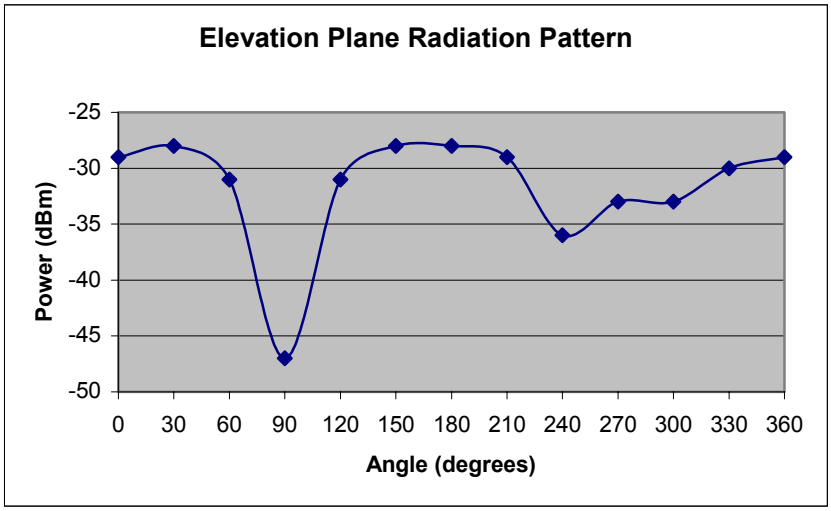

Figure 5.16. Elevation plane radiation pattern measured in outdoor range.

Table 5.6. Simulated and Measured Antenna Performance Comparison.

Antenna Characteristics	Simulated	Measured	Error
Frequency of Minimum S11 (GHz)	2.2155	2.21	-0.01
Frequency of Minimum Axial Ratio (GHz)	2.2155	2.217	0.002
Impedance Bandwidth (MHz)	133	235	102
Minimum Axial Ratio (dB)	0.1	1.7	1.6
Azimuth Radiation Pattern Ripple (dB)	1	3	-2
Azimuth Axial Ratio Ripple (dB)	1	3	-2
Elevation Beamwidth (degrees)	180	120 and 110	-60 and -70
Elevation Axial Ratio 6 dB Beamwidth (degrees)	140	135 and 105	-5 and -35

The impedance bandwidth shows the largest performance discrepancy between the measured and simulated data. This discrepancy may be a result of the fact that the simulated antenna was designed using a feed network consisting of 50 ohm microstrip transmission lines connected to the input of each antenna element, while the fabricated and tested antenna used 100 ohm lines. As mentioned earlier, the 100 ohm lines provided a simpler design because they did not required a quarterwave matching section at the first set of T-junctions in the corporate feed network. Since the 100 ohm transmission line has an impedance nearer to that of the antenna's input impedance, this may be why the impedance bandwidth is larger for the fabricated case.

The ripple in both the radiation azimuth pattern and axial ratio azimuth pattern is greater than the simulated case. A portion of the error is likely a result of the movement of the rotating platform. During the measurement of the patterns using the spectrum analyzer, the received signal was very sensitive to movement in the cables and antenna platform. The largest source of error in the measurement is probably due to multipath from the ground reflections. These errors are expected to have a greater influence for the axial ratio measurements because any reflected signals will experience a slight change in polarization. Therefore, the measured electric fields at 0, 45, 90, and 135 degrees will not directly correspond to the polarizations of the dipole antenna's electric fields at these same degrees.